JOURNAL OF SPACECRAFT AND ROCKETS
Vol. 43, No. 1, January–February 2006

Influences of Electrical Conductivity of Wall on Magnetohydrodynamic Control of Aerodynamic Heating

Takayasu Fujino*
University of Tsukuba, Tsukuba 305-8573, Japan
Hiroyuki Sugita,† Masahito Mizuno,‡ and Ikkoh Funaki§
Japan Aerospace Exploration Agency, Tokyo 182-8522, Japan
and
Motoo Ishikawa¶
University of Tsukuba, Tsukuba 305-8573, Japan

Influences of the electrical conductivity of the wall of a space vehicle on the control of the aerodynamic heating in Earth-reentry flight by applying the magnetic field are numerically examined using an axisymmetric two-dimensional (*r–z*) thermochemical nonequilibrium magnetohydrodynamic computational fluid dynamics code. Numerical results show that when the wall of an axisymmetric blunt body is assumed to be an insulating wall, applying a dipole-type magnetic field with *r* and *z* components pushes the bow shock wave away from the blunt body and reduces the aerodynamic heating. On the other hand, when the wall is assumed to be a conducting wall, the aerodynamic heating cannot be reduced by applying the magnetic field. This is because the strong Hall electric field on the *r–z* plane cannot be obtained in the case of the conducting wall, so that the large electric current density in the azimuthal direction cannot be obtained and the shock wave cannot be pushed away from the blunt body.

Nomenclature

$\boldsymbol{B}$	=	magnetic field vector
B_r, B_z	=	components of magnetic flux density in the r and z directions
B_0	=	magnetic flux density at stagnation point
D_s	=	effective diffusion coefficient of species s
$\hat{D}_s$	=	average vibrational energy of molecule s, which is created or destroyed at rate $\dot{\omega}_s$
E	=	total energy
$\boldsymbol{E}$	=	electric field vector
E_r, E_z	=	components of electric field in the r and z directions
e	=	electronic charge
$\boldsymbol{e}_r$, $\boldsymbol{e}_z$	=	unit vectors in r and z directions
$e_{\mathrm{ve},s}$	=	vibrational-electronic-electron energy of species s
$e^*_{v,s}$	=	equilibrium vibrational energy of species s
H	=	total enthalpy
h_s	=	enthalpy of species s
$h_{\mathrm{ve},s}$	=	vibrational-electronic-electron enthalpy of species s
I_s	=	first ionization energy of species s
$\boldsymbol{J}$	=	vector of electric current density
J_r, J_θ, J_z	=	components of electric current density in the r, θ, and z directions
k_b	=	Boltzmann's constant
$k_{f,r}$, $k_{b,r}$	=	forward and backward reaction-rate coefficients for reaction r
M_e	=	molecular weight of electron
M_s	=	molecular weight of species s
m_e	=	mass of electron
n_e	=	electron number density
$\dot{n}_{e,s}$	=	molar rate of production of species s by electron impact ionization
p	=	static pressure
p_e	=	partial pressure of electron
p_s	=	partial pressure of species s
R	=	universal gas constant
R_b	=	nose radius of Orbital Reentry Experiments
$R_{f,r}$, $R_{b,r}$	=	forward and backward reaction rates for reaction r
r, θ, z	=	cylindrical coordinates
T_{tr}	=	translational-rotational temperature
T_{ve}	=	vibrational-electronic-electron temperature
t	=	time
u_r, u_θ, u_z	=	velocity components in the r, θ, and z directions
y_s	=	mole fraction of species s
$\alpha_{s,r}$, $\beta_{s,r}$	=	forward and backward stoichiometric coefficients of species s in reaction r
β	=	electron Hall parameter
ϵ_0	=	permittivity in vacuum
η_{tr}	=	mixture translational-rotational thermal conductivity
η_{ve}	=	mixture vibrational-electron thermal conductivity
μ	=	mixture viscosity
$\nu_{e,s}$	=	effective energy exchange collision frequency of electron with species s
ξ, η	=	generalized curvilinear coordinates
ρ	=	total mass density
ρ_s	=	mass density of species s
σ	=	electrical conductivity
$\sigma_{e,s}$	=	effective energy exchange cross section of electrons with neutral species s
$\tau_{i,j}$	=	viscous shear stress
τ_s	=	translational-vibrational energy relaxation time of species s
ϕ	=	electric potential

Received 1 October 2004; revision received 15 June 2005; accepted for publication 20 June 2005.

*Assistant Professor, Graduate School of Systems and Information Engineering. Member AIAA.
†Associate Senior Engineer, Space Systems Evaluation Engineering Group, Institute of Space Technology and Aeronautics. Member AIAA.
‡Scientist, High Enthalpy Wind Tunnel Team, Wind Tunnel Technology Center, Institute of Space Technology and Aeronautics.
§Associate Professor, Institute of Space and Aeronautical Science. Member AIAA.
¶Professor, Graduate School of Systems and Information Engineering. Senior Member AIAA.

ω_s = mass production rate of species s
$\dot{\omega}_{ve}$ = production rate of vibrational-electronic-electron energy

I. Introduction

THE blunt-body Orbital Reentry Experiments (OREX) were launched by the H-II rocket from Tanegashima Space Center of Japan in 1994 to conduct reentry experiments.[1] The experiments were successfully conducted, and the data related to the aerodynamic heating were acquired, which reconfirmed that the development of thermal protection techniques was very important to improve manned reusable space vehicles. As one of thermal protection techniques in reentry flights, the flow control by applying a magnetic field, which is called magnetohydrodynamic (MHD) control, was proposed in the 1950s (for example, see Refs. 2–4). The idea of the MHD control is that the Lorentz force, which is induced by applying the magnetic field to a weakly ionized plasma flow in the shock layer, decelerates the flow velocity in the shock layer and pushes the bow shock wave away from a space vehicle. Consequently, the convective aerodynamic heating can be reduced by the MHD control. On the other hand, in the 1950s, the concept of the MHD control was not considered to be realistic because a very large and heavy magnet system was required to produce the strong magnetic field enough to control the flow in the shock layer. However, a considerable development of magnet technology with a superconducting magnet has been shown in more than a half-century since the concept of the MHD control was proposed. For example, a system of thin superconducting solenoid magnet with the total weight of 380 kg and the central magnetic field strength of about 1.2T (coil diameter, 0.9 m; coil length, 1.4 m) was constructed for the balloon-borne experiment with a superconducting spectrometer to measure the energy spectrum of cosmic-ray antiprotons (the Bess-Polar program[5]). The considerable development of the magnet system technology in these days encourages us to reconsider the MHD control.

The authors conducted a numerical study for examining the possibility of the MHD control under the real reentry flight conditions of OREX at an altitude of about 60 km, where the aerodynamic heating was maximum in the OREX trajectory.[6] For the numerical study, we developed an axisymmetric two-dimensional thermochemical nonequilibrium Navier–Stokes MHD computational fluid dynamics (CFD) code. The numerical results indicated that the MHD control could reduce the aerodynamic heating under the real reentry flight conditions and also that the consideration of the thermochemical reactions and the nonuniformity of the electrical conductivity in the shock layer was very important for examining the possibility and usefulness of the MHD control. The numerical study, however, neglected the Hall effect for simplicity.

Porter and Cambel[7] examined the influences of the Hall effect on the MHD control by means of a local similarity solution. The obtained results showed that the Hall effect tended to reduce the usefulness of the MHD control, and also that when the Hall effect was considered, the electrical conductivity of the wall of a body influenced the MHD control because the electrical conductivity of the wall affected the electric field and the electric current, which were induced by the Hall effect. The similarity solution, however, was carried out on the assumptions of inviscid and constant property in the shock layer. Furthermore, the similarity solution could not clear the MHD field in all over the shock layer in front of the body because the similarity solution could analyze only the MHD field in the vicinity of the stagnation point.

Lineberry et al.[8] recently conducted numerical simulations on the MHD flow around a test body in their experimental facility. The numerical simulations employed the two-dimensional full Navier–Stokes equations including a finite-rate chemical kinetics model of air and the low-magnetic-Reynolds-number model including the Hall effect. The numerical results clearly showed that the Hall effect and the nonuniformity of plasma properties influenced the MHD control. The influences of the electrical conductivity of the wall of the body on the MHD control, however, were not examined in the numerical simulations.

The purpose of the present numerical study, therefore, is to examine the influences of the electrical conductivity of the wall of a space vehicle on the MHD control by using a newly developed axisymmetric two-dimensional thermochemical nonequilibrium MHD CFD code, which can consider the Hall effect. The numerical simulations are carried out under the reentry flight conditions of OREX at the altitude of about 60 km and under the two electrical wall conditions: the insulating wall and the conducting wall.

II. Numerical Method and Numerical Condition

A. OREX Configuration and Flight Conditions

Figure 1 shows the configuration of OREX.[1] The forebody shape is composed of a spherical nose with a radius of 1.35 m, a cone, and a circular shoulder. The freestream pressure, the freestream temperature, and the freestream velocity are 23.6 Pa, 248.1 K, and 5562 m/s, respectively, in the present numerical simulations; these freestream conditions correspond to the freestream conditions at the altitude of about 60 km in the OREX reentry experiments.[1]

Figure 2 shows an externally applied magnetic field in the vicinity of OREX. The externally applied magnetic field is assumed to be produced by a dipole magnet placed at the point of $r = 0$ and $z = 0$ inside OREX:

$$\boldsymbol{B} = -\frac{B_0 R_b^3}{2(z^2+r^2)^{\frac{3}{2}}}\left[\left(\frac{2z^2}{z^2+r^2}-\frac{r^2}{z^2+r^2}\right)\boldsymbol{e}_z + \frac{3zr}{z^2+r^2}\boldsymbol{e}_r\right] \quad (1)$$

In the present study, B_0 is set to 0.5 T. It is possible that we use a permanent magnet for applying a magnetic field of about 0.5 T in an experimental demonstration of the present study using a ground test facility if the duration time in the experiment is short. Takizawa et al.[9] have experimentally examined influences of applying the magnetic field on the shock layer around a test body, where a permanent magnet of about 0.4 T is installed, using a small arc-heater ground test facility.

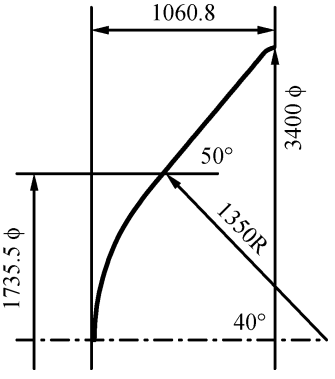

Fig. 1 OREX configuration (unit: millimeters).

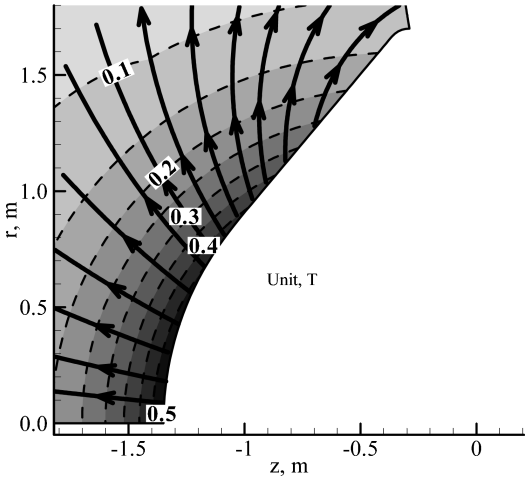

Fig. 2 Distribution of externally applied magnetic field.

B. Basic Equations

We regard the flowfield and the electromagnetic field around OREX as axisymmetric two-dimensional field (r–z).

1. Gasdynamics

The basic equations for the gasdynamics are the mass conservation equations of chemical species, the momentum conservation equations, the total energy conservation equation, and the vibrational-electronic-electron energy conservation equation. We consider the following 11 chemical species: N, O, N_2, O_2, NO, N^+, O^+, N_2^+, O_2^+, NO^+, and e^-. As a finite-rate chemical kinetics model, we use Dunn-and-Kang's model,[10] in which 32 chemical reactions are included. Park's two-temperature model[11] is employed to take account of the thermal nonequilibrium state. The basic equations for the gasdynamics are written as follows.

Mass conservation equations of chemical species (s = N, O, N_2, O_2, NO, N^+, O^+, N_2^+, O_2^+, NO^+, e^-):

$$\frac{\partial \rho_s}{\partial t} + \frac{\partial}{\partial r}(\rho_s u_r) + \frac{\partial}{\partial z}(\rho_s u_z) = \dot{\omega}_s + \frac{\partial}{\partial r}\left(\rho D_s \frac{\partial y_s}{\partial r}\right) + \frac{\partial}{\partial z}\left(\rho D_s \frac{\partial y_s}{\partial z}\right) - \frac{1}{r}\left(\rho_s u_r - \rho D_s \frac{\partial y_s}{\partial r}\right) \tag{2}$$

where the total mass density ρ is given by

$$\rho = \sum_s \rho_s \tag{3}$$

The first term $\dot{\omega}_s$ on the right-hand side of Eq. (2) is the source term for the mass production rate of species s and is expressed as

$$\dot{\omega}_s = M_s \sum_{r=1}^{32} (\beta_{s,r} - \alpha_{s,r})(R_{f,r} - R_{b,r}) \tag{4}$$

The forward and backward reaction rates $R_{f,r}$ and $R_{b,r}$ are, respectively, defined by

$$R_{f,r} = k_{f,r} \prod_{s=1}^{11} \left(\frac{\rho_s}{M_s}\right)^{\alpha_{s,r}}, \qquad R_{b,r} = k_{b,r} \prod_{s=1}^{11} \left(\frac{\rho_s}{M_s}\right)^{\beta_{s,r}} \tag{5}$$

where the forward reaction-rate coefficients $k_{f,r}$ and the backward reaction-rate coefficients $k_{b,r}$ are tabulated in Refs. 10 and 12.

Momentum conservation equations:

$$\frac{\partial \rho u_r}{\partial t} + \frac{\partial}{\partial r}\left(\rho u_r^2 + p\right) + \frac{\partial}{\partial z}(\rho u_r u_z) = \frac{\partial \tau_{rr}}{\partial r} + \frac{\partial \tau_{rz}}{\partial z} + J_\theta B_z - \frac{1}{r}\left[\rho\left(u_r^2 - u_\theta^2\right) - \tau_{rr} + \tau_{\theta\theta}\right] \tag{6}$$

$$\frac{\partial \rho u_\theta}{\partial t} + \frac{\partial}{\partial r}(\rho u_\theta u_r) + \frac{\partial}{\partial z}(\rho u_\theta u_z) = \frac{\partial \tau_{r\theta}}{\partial r} + \frac{\partial \tau_{z\theta}}{\partial z} + J_z B_r - J_r B_z - \frac{2}{r}(\rho u_r u_\theta - \tau_{r\theta}) \tag{7}$$

$$\frac{\partial \rho u_z}{\partial t} + \frac{\partial}{\partial r}(\rho u_z u_r) + \frac{\partial}{\partial z}\left(\rho u_z^2 + p\right) = \frac{\partial \tau_{rz}}{\partial r} + \frac{\partial \tau_{zz}}{\partial z} - J_\theta B_r - \frac{1}{r}(\rho u_r u_z - \tau_{rz}) \tag{8}$$

where the static pressure p and the viscous stress terms $\tau_{i,j}$ are defined by

$$p = \sum_s p_s = \sum_{s=1-10} \rho_s \frac{\bar{R}}{M_s} T_{\mathrm{tr}} + \rho_e \frac{\bar{R}}{M_e} T_{\mathrm{ve}} \tag{9}$$

$$\tau_{rr} = \frac{2}{3}\mu\left(2\frac{\partial u_r}{\partial r} - \frac{\partial u_z}{\partial z} - \frac{u_r}{r}\right), \quad \tau_{\theta\theta} = \frac{2}{3}\mu\left(2\frac{u_r}{r} - \frac{\partial u_r}{\partial r} - \frac{\partial u_z}{\partial z}\right)$$

$$\tau_{zz} = \frac{2}{3}\mu\left(2\frac{\partial u_z}{\partial z} - \frac{\partial u_r}{\partial r} - \frac{u_r}{r}\right), \quad \tau_{r\theta} = \tau_{\theta r} = \mu\left(\frac{\partial u_\theta}{\partial r} - \frac{u_\theta}{r}\right)$$

$$\tau_{rz} = \tau_{zr} = \mu\left(\frac{\partial u_r}{\partial z} + \frac{\partial u_z}{\partial r}\right), \quad \tau_{\theta z} = \tau_{z\theta} = \mu\frac{\partial u_\theta}{\partial z} \tag{10}$$

Total energy conservation equation:

$$\frac{\partial \rho E}{\partial t} + \frac{\partial}{\partial r}(\rho H u_r) + \frac{\partial}{\partial z}(\rho H u_z) = \frac{\partial}{\partial r}\left(\eta_{\mathrm{tr}}\frac{\partial T_{\mathrm{tr}}}{\partial r} + \eta_{\mathrm{ve}}\frac{\partial T_{\mathrm{ve}}}{\partial r}\right) + \frac{\partial}{\partial z}\left(\eta_{\mathrm{tr}}\frac{\partial T_{\mathrm{tr}}}{\partial z} + \eta_{\mathrm{ve}}\frac{\partial T_{\mathrm{ve}}}{\partial z}\right) + \frac{\partial}{\partial r}\left(\rho\sum_s h_s D_s \frac{\partial y_s}{\partial r}\right) + \frac{\partial}{\partial z}\left(\rho\sum_s h_s D_s \frac{\partial y_s}{\partial z}\right) + \frac{\partial}{\partial r}(\tau_{rr}u_r + \tau_{\theta r}u_\theta + \tau_{zr}u_z) + \frac{\partial}{\partial z}(\tau_{rz}u_r + \tau_{\theta z}u_\theta + \tau_{zz}u_z) + J_r E_r + J_z E_z - \frac{\rho H u_r}{r} + \frac{\rho}{r}\sum_s h_s D_s \frac{\partial y_s}{\partial r} + \frac{1}{r}\left(\eta_{\mathrm{tr}}\frac{\partial T_{\mathrm{tr}}}{\partial r} + \eta_{\mathrm{ve}}\frac{\partial T_{\mathrm{ve}}}{\partial r}\right) + \frac{1}{r}(\tau_{rr}u_r + \tau_{\theta r}u_\theta + \tau_{zr}u_z) \tag{11}$$

where the total enthalpy H is defined as

$$H = E + \frac{p}{\rho} \tag{12}$$

Vibrational-electronic-electron energy conservation equation:

$$\frac{\partial \rho e_{\mathrm{ve}}}{\partial t} + \frac{\partial}{\partial r}(\rho e_{\mathrm{ve}} u_r) + \frac{\partial}{\partial z}(\rho e_{\mathrm{ve}} u_z) = \dot{\omega}_{\mathrm{ve}} + \frac{\partial}{\partial r}\left(\eta_{\mathrm{ve}}\frac{\partial T_{\mathrm{ve}}}{\partial r}\right) + \frac{\partial}{\partial z}\left(\eta_{\mathrm{ve}}\frac{\partial T_{\mathrm{ve}}}{\partial z}\right) + \frac{\partial}{\partial r}\left(\rho\sum_s h_{\mathrm{ve},s} D_s \frac{\partial y_s}{\partial r}\right) + \frac{\partial}{\partial z}\left(\rho\sum_s h_{\mathrm{ve},s} D_s \frac{\partial y_s}{\partial z}\right) + \frac{J_r^2 + J_\theta^2 + J_z^2}{\sigma} - \frac{1}{r}\left(\rho e_{\mathrm{ve}} u_r - \rho\sum_s h_{\mathrm{ve},s} D_s \frac{\partial y_s}{\partial r} - \eta_{\mathrm{ve}}\frac{\partial T_{\mathrm{ve}}}{\partial r}\right) \tag{13}$$

where $\dot{\omega}_{\mathrm{ve}}$ is expressed as

$$\dot{\omega}_{\mathrm{ve}} = \sum_{s=mol} \rho_s \frac{e_{v,s}^* - e_{v,s}}{< \tau_s >} + 2\rho\frac{3}{2}\bar{R}(T_{\mathrm{tr}} - T_{\mathrm{ve}})\sum_{s\neq e}\frac{\nu_{e,s}}{M_s} - \sum_{s=ion}\dot{n}_{e,s} I_s + \sum_{s=mol}\dot{\omega}_s \hat{D}_s - p_e\left(\frac{\partial u_r}{\partial r} + \frac{\partial u_z}{\partial z} + \frac{u_r}{r}\right) \tag{14}$$

where the relaxation time of each species for a translational-vibrational energy relaxation τ_s is calculated from the sum of the relaxation time formula proposed by Millikan and White[13] and the correction term suggested by Park.[11] The average vibrational energy $\hat{D}_s$, which is created or destroyed at the rate $\dot{\omega}_s$, is computed by using the nonpreferential model.[12] The transport coefficients such as the effective diffusion coefficient of each species D_s, the mixture viscosity μ, the mixture translational-rotational thermal conductivity η_{tr}, and the mixture vibrational-electron thermal conductivity η_{ve} are estimated by an extension model of Yos's formulas to the multitemperature gas mixture (see Ref. 12). The model has some inaccuracy

for the flowfield with the ionization, but the major feature of the flowfield with the MHD control is determined by the shock wave and the electric current distribution. And therefore, the inaccuracy would not result in a large modification of the flowfield with the MHD control.

2. Electrodynamics

The basic equations used for the electrodynamics are the steady Maxwell equations and the generalized Ohm's law including the Hall effect. The magnetic Reynolds number is less than unity under the present numerical conditions, and then we neglect the induced magnetic field. The basic equations for the electrodynamics are written as follows.

Maxwell equations:

$$\nabla \times \boldsymbol{E} = 0 \tag{15}$$

$$\nabla \cdot \boldsymbol{J} = 0 \tag{16}$$

Generalized Ohm's law:

$$\begin{pmatrix} J_r \\ J_\theta \\ J_z \end{pmatrix} = \frac{\sigma}{1+\beta^2} \begin{pmatrix} 1+m^2B_r^2 & -mB_z & m^2B_rB_z \\ mB_z & 1 & -mB_r \\ m^2B_rB_z & mB_r & 1+m^2B_z^2 \end{pmatrix} \begin{pmatrix} E_r + u_\theta B_z + \dfrac{1}{en_e}\dfrac{\partial p_e}{\partial r} \\ u_z B_r - u_r B_z \\ E_z - u_\theta B_r + \dfrac{1}{en_e}\dfrac{\partial p_e}{\partial z} \end{pmatrix}, \qquad m = \frac{\beta}{|\boldsymbol{B}|} \tag{17}$$

where the electrical conductivity σ and the Hall parameter β are, respectively, expressed as

$$\sigma = \frac{n_e e^2}{m_e \sum_{s \neq e} \nu_{e,s}}, \qquad \beta = \frac{e|\boldsymbol{B}|}{m_e \sum_{s \neq e} \nu_{e,s}} \tag{18}$$

The effective energy-exchange collision frequency $\nu_{e,s}$ of electrons with the other chemical species s is written as

$$\nu_{e,s} = \begin{cases} 6\pi \left(\dfrac{e^2}{12\pi\epsilon_0 k_b T_{\mathrm{ve}}}\right)^2 \times \ell_n \left[12\pi \left(\dfrac{\epsilon_0 k_b}{e^2}\right)^{\frac{3}{2}} \sqrt{\dfrac{T_{\mathrm{ve}}^3}{n_e}}\right] n_s \sqrt{\dfrac{8k_b T_{\mathrm{ve}}}{\pi m_e}} & \text{if } s \text{ is ion species} \\ \dfrac{4}{3}\sigma_{e,s} n_s \sqrt{\dfrac{8k_b T_{\mathrm{ve}}}{\pi m_e}} & \text{otherwise} \end{cases} \tag{19}$$

where $\sigma_{e,s}$ represents the effective energy exchange cross section of electrons with the neutral species and is computed using the curve fit presented in Ref. 12.

C. Numerical Procedure

Figure 3 illustrates a computational grid. The number of grid points is 65 in the ξ direction along the wall surface and 250 in the outward η direction. Because the prediction of the heat flux on the wall surface is extremely sensitive to the grid near the wall surface, we checked the grid dependency in advance. Based on the check, we set the minimum mesh size near the wall surface to about 2 μm.

The conservation equations of the gasdynamics are transformed into the generalized curvilinear coordinate system. The convection terms are calculated by the advection upstream splitting method (AUSM)-DV scheme[14] coupled with the fourth-order compact MUSCL-TVD scheme (FCMT).[15] The viscous terms are calculated by the second-order central-differencing scheme.

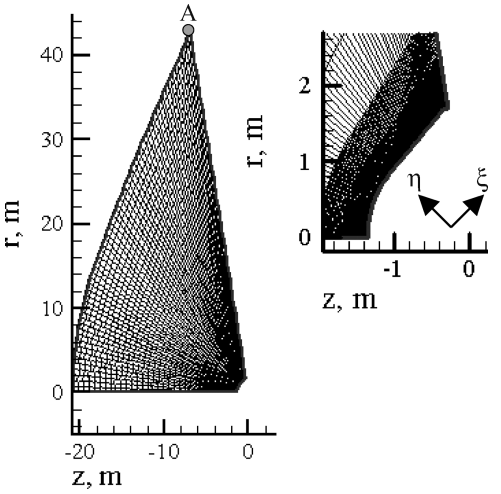

Fig. 3 Computational grid.

The time integration is performed by the lower–upper symmetric Gauss–Seidel (LU-SGS) scheme[16] coupled with the diagonal point implicit scheme.[17] We use the no-slip wall condition, the fixed wall temperature condition, and the noncatalytic wall condition on the wall boundary. The wall temperature is set to 1519 K; this value corresponds to the wall temperature at the stagnation point estimated at the altitude of about 60 km in the OREX reentry experiments. The translational-rotational temperature T_{tr} and the vibrational-electronic-electron temperature T_{ve} on the wall boundary are assumed to be equilibrium with the wall temperature. We derive a second-order elliptic partial differential equation on the electric potential ϕ from Eqs. (15–17). The equation is solved by the Galerkin finite element method under the insulating wall condition and the conducting wall condition to examine the influences of the electrical conductivity of the wall on the MHD control. In the case of the insulating wall condition, the normal component of electric current density J_n on the wall surface and the other boundaries in Fig. 3 is set to 0 A/m^2, while the electric potential ϕ at the point A in Fig. 3 is set to 0 V for establishing a reference value of electric potential. In the case of the conducting wall condition, the electric potential ϕ on the wall surface is set to 0 V. On the other boundaries in Fig. 3, the normal component of electric current density J_n is set to 0 A/m^2.

We obtain converged solutions by continuing calculations until the L_2 norms of the conservation equations for gasdynamics reach 10^{-4}. As shown in Ref. 6, we compared shock location of both numerical results and experimental data in Lobb's experiments[18] to validate the reliability of the numerical solutions as for the gasdynamics part. As a result, good agreement between numerical results and experimental data was obtained. We also confirmed by comparing the numerical results and experimental data in MHD power generation experiments with a large-scale generator "Sakhalin" that the reliability of the numerical solutions as for the electrodynamics part is very high.[19]

III. Results and Discussion

Figure 4 depicts two-dimensional distributions of the static pressure normalized by the dynamic pressure of the freestream for the three cases: without the magnetic field (case 1), with the magnetic field under the insulating wall condition (case 2), and with the magnetic field under the conducting wall condition (case 3). Figure 5 shows distributions of the translational-rotational temperature T_{tr} (solid line) and the vibrational-electronic-electron temperature T_{ve} (dashed line) along the stagnation line for the three cases. These figures show that the bow shock wave is pushed away from OREX by applying the magnetic field under the insulating wall condition. On the other hand, under the conducting wall condition there is little effect of applying the magnetic field on the flowfield, and the position of the bow shock wave is almost the same as that without the magnetic field. As can be seen from Fig. 5, the increase of the shock

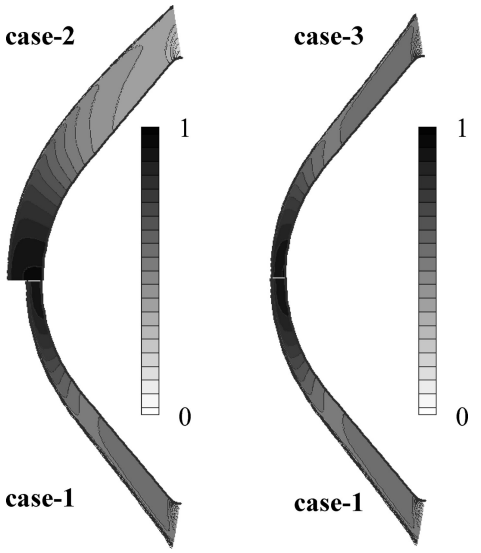

Fig. 4 Two-dimensional distributions of static pressure normalized by dynamic pressure of freestream for the three cases: without magnetic field (case 1), with magnetic field under insulating wall condition (case 2), and with magnetic field under conducting wall condition (case 3).

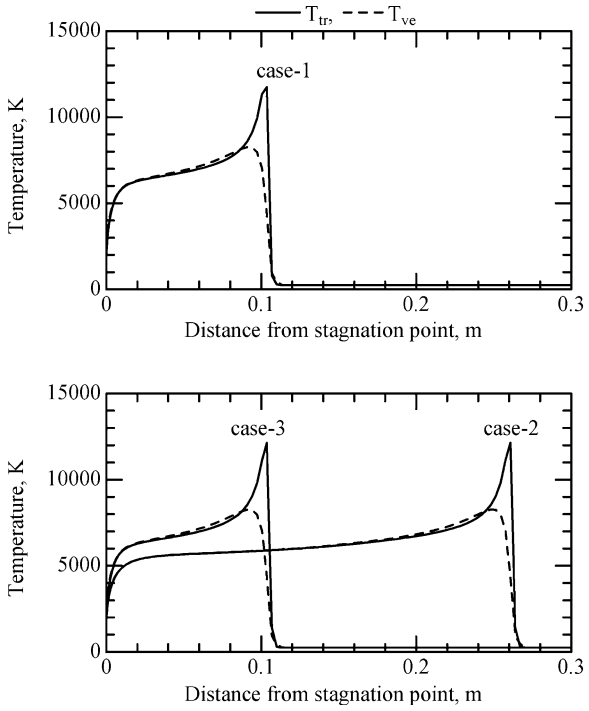

Fig. 5 Distributions of translational-rotational temperature T_{tr} (——) and vibrational-electronic-electron temperature T_{ve} (– – –) along the stagnation line without magnetic field (case 1), with magnetic field under insulating wall condition (case 2), and with magnetic field under conducting wall condition (case 3).

standoff distance along the stagnation line under the insulating wall condition is about 15 cm.

Figure 6 depicts distributions of the electrical conductivity along the stagnation line with the magnetic field under the insulating wall condition and with the magnetic field under the conducting wall condition. Under any wall conditions, the electrical conductivity is about 115 S/m behind the bow shock wave, and then it decreases from about 115 to 0 S/m toward the stagnation point. Figure 7 shows distributions of the electron Hall parameter along the stagnation line with the magnetic field under the insulating wall condition and with the magnetic field under the conducting wall condition. Under any wall conditions, the electron Hall parameter in the shock layer is larger than unity and is about 10–15.

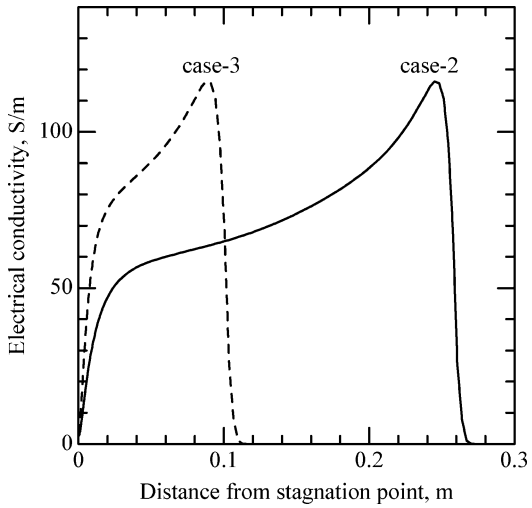

Fig. 6 Distributions of electrical conductivity along the stagnation line with magnetic field under insulating wall condition (case 2) and with magnetic field under conducting wall condition (case 3).

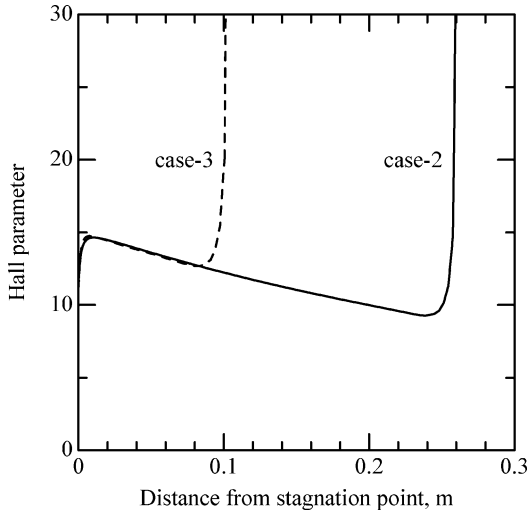

Fig. 7 Distributions of electron Hall parameter along the stagnation line with magnetic field under insulating wall condition (case 2) and with magnetic field under conducting wall condition (case 3).

Figure 8 depicts two-dimensional distributions of the Hall electric potential on the r–z plane with the magnetic field under the insulating wall condition and with the magnetic field under the conducting wall condition. Under the insulating wall condition, the Hall electric potential builds up toward the shoulder of OREX along the wall. The difference of the Hall electric potential between the stagnation point and the shoulder of OREX is about 4000 V. Thus, the insulating wall condition leads to producing the strong Hall electric field in the shock layer. On the other hand, the strength of the Hall electric field in the shock layer under the conducting wall condition is considerably weaker than that under the insulating wall condition.

Figure 9 illustrates two-dimensional distributions of the azimuthal component of electric current density with the magnetic field under the insulating wall condition and with the magnetic field under the conducting wall condition. The Lorenz force induced by the interaction between the azimuthal component of electric current and the magnetic field decelerates the flow in the shock layer and pushes the bow shock wave away from OREX. As can be seen from Fig. 9, the azimuthal components of electric current density in the shock layer under the conducting wall condition is significantly smaller than that under the insulating wall condition. This is because the strength of the Hall electric field under the conducting wall condition is considerably weaker than that under the insulating wall

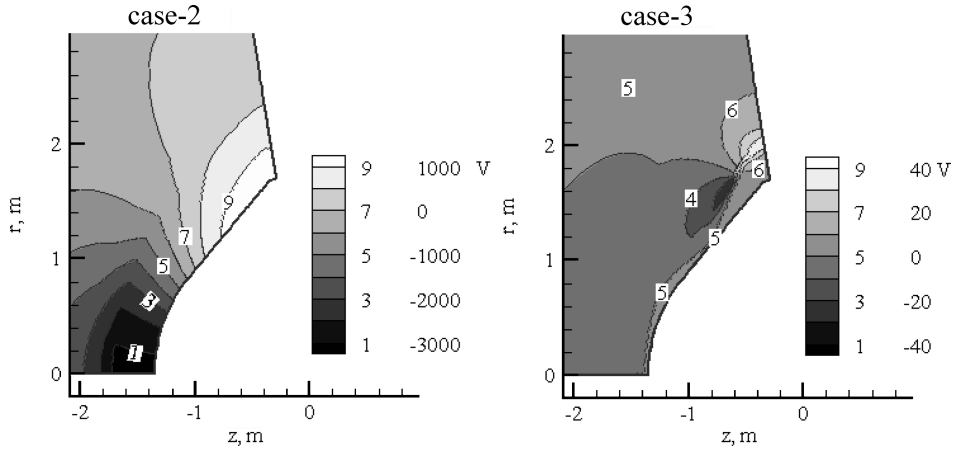

Fig. 8 Two-dimensional distributions of Hall electric potential on the *r–z* plane with magnetic field under insulating wall condition (case 2) and with magnetic field under conducting wall condition (case 3).

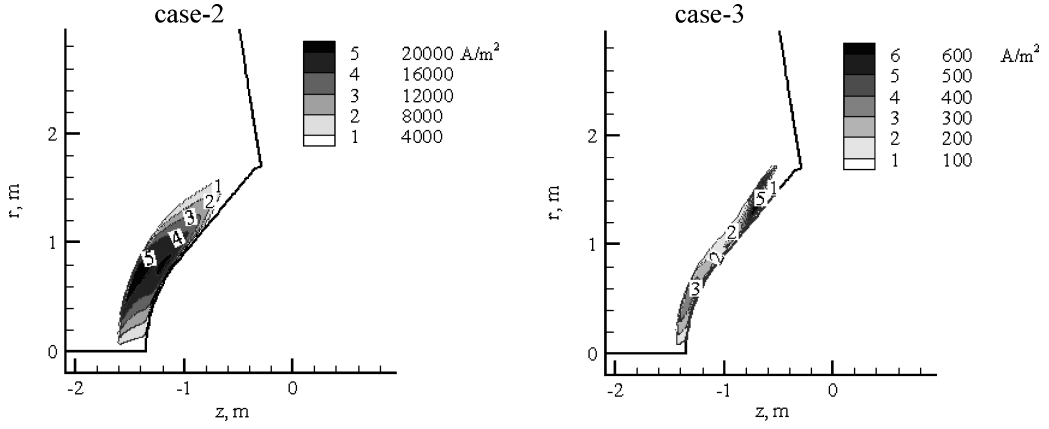

Fig. 9 Two-dimensional distributions of azimuthal component of electric current density with magnetic field under insulating wall condition (case 2) and with magnetic field under conducting wall condition (case 3).

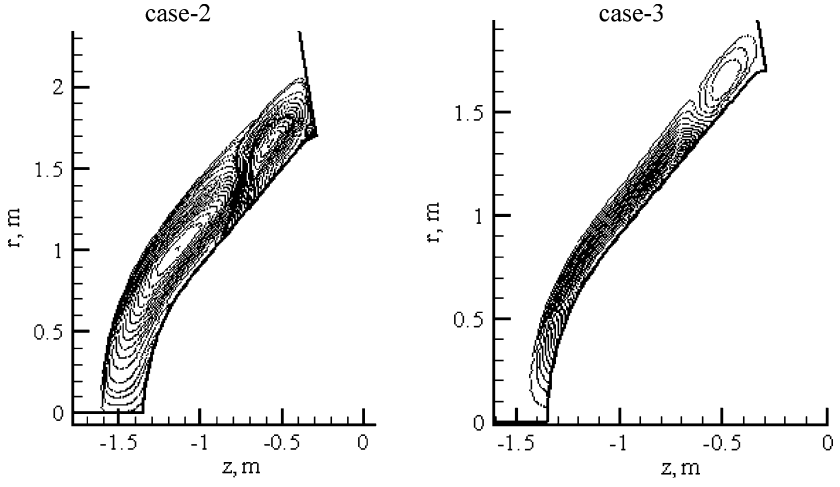

Fig. 10 Streamlines of electric current on the *r–z* plane with magnetic field under insulating wall condition (case 2) and with magnetic field under conducting wall condition (case 3).

condition, as shown in Fig. 8. The considerable difference in the azimuthal component of electric current density between the two wall conditions leads to that the shock wave can be pushed away from OREX by applying the magnetic field under the insulating wall condition, whereas it cannot be pushed under the conducting wall condition, as shown in Figs. 4 and 5.

Figure 10 depicts streamlines of the electric current on the *r–z* plane with the magnetic field under the insulating wall condition and with the magnetic field under the conducting wall condition. Under the insulating wall condition, the electric current has eddy-like paths on the *r–z* plane and runs through neither the wall nor the bow shock wave. The rotational direction of the eddy-like electric current on the stagnation-line side is clockwise, and the rotational direction on the shoulder side is counterclockwise. Under the conducting wall condition, the electric current flows toward the shoulder side in the shock layer and then runs through the wall. Thus, there are

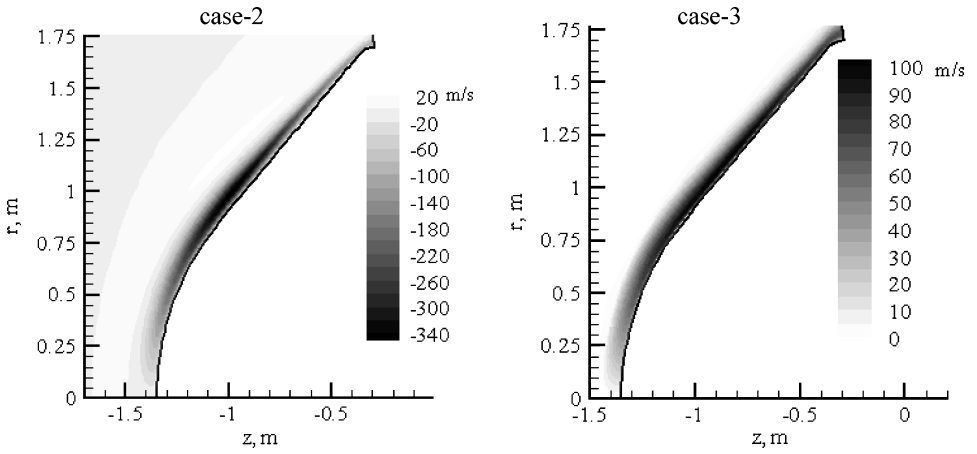

Fig. 11 Two-dimensional distributions of flow velocity in the azimuthal direction with magnetic field under insulating wall condition (case 2) and with magnetic field under conducting wall condition (case 3).

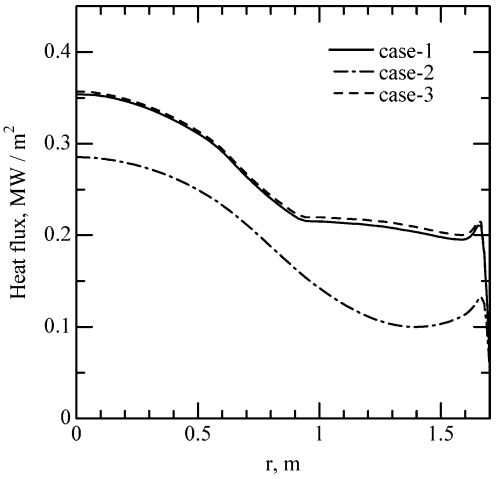

Fig. 12 Distributions of heat flux along the wall surface for the three cases: without magnetic field (case 1), with magnetic field under insulating wall condition (case 2), and with magnetic field under conducting wall condition (case 3).

electric current paths between the plasma in the shock layer and the wall. Therefore, under the conducting wall condition the strong Hall electric field cannot be obtained in the shock layer.

Figure 11 presents two-dimensional distributions of the flow velocity in the azimuthal direction with the magnetic field under the insulating wall condition and with the magnetic field under the conducting wall condition. The interaction between the electric current on the r–z plane and the magnetic field induces the azimuthal component of the flow velocity. Under any wall conditions, the velocity in the azimuthal direction with the absolute value of the order of 10^2 m/s arises near the wall where the magnetic field is strong. The direction of the flow velocity in the azimuthal direction near the wall, however, becomes opposite under the two wall conditions. This is because the direction of the electric current on the r–z plane near the wall is opposite under the two wall conditions, as shown in Fig. 10.

Figure 12 depicts distributions of the heat flux along the wall surface for the three cases: without the magnetic field, with the magnetic field under the insulating wall condition, and with the magnetic field under the conducting wall condition. Under the insulating wall condition, applying the magnetic field significantly reduces the heat flux on all over the wall surface. The heat flux at the stagnation point with the magnetic field under the insulating wall condition is about 82% of its value without the magnetic field, and the amount of the total aerodynamic heating, which is calculated by integrating the heat flux over the wall surface, is about 70% of its value without the magnetic field. On the other hand, under the conducting wall condition where there is little effect of applying the magnetic field on the flowfield as shown in Figs. 4 and 5, the distribution of the heat flux along the wall surface is nearly the same as that without the magnetic field. Thus, under the conducting wall condition applying the magnetic field is not useful for controlling the flowfield and reducing the aerodynamic heating.

As just shown, we have numerically demonstrated that the electrical conductivity of the wall significantly influences the possibility of the MHD control, and if the wall is the insulating wall, applying the magnetic field of about 0.5 T can reduce the amount of the total aerodynamic heating by about 70% of that obtained without applying the magnetic field. We think that the reduction ratio is very large, and the concept of the MHD control is very attractive.

In the present study, the ion slip term in the generalized Ohm's law is neglected for simplicity. From the values of the electron Hall parameter in Fig. 7, the ion Hall parameter is estimated at the order of 0.1, and so the product of electron and ion Hall parameters, which is commonly referred to as the ion slip parameter, is estimated at the order of 1. Thus, the absolute value of the ratio of the ion slip term to the Hall-effect term in the generalized Ohm's law is estimated at the order of 0.1 for the present numerical flight conditions. We, therefore, think that the ion slip phenomenon does not make considerable differences from the numerical results obtained in the present study, where the ion slip effect is neglected.

IV. Conclusions

The influences of the electrical conductivity of the wall (insulating wall, conducting wall) on the control of the aerodynamic heating by the MHD technology have been numerically studied by using the axisymmetric two-dimensional r–z thermochemical nonequilibirum MHD CFD code, which can consider the Hall effect. The numerical simulations have been conducted under the flight conditions at the altitude of about 60 km in the reentry flight experiments with the axisymmetric blunt-body OREX. The magnetic field with r and z components has been assumed to be produced by a dipole magnet placed inside OREX. The magnetic flux density at the stagnation point has been set to 0.5 T.

Numerical results have demonstrated that if the insulating wall can be realized, the strong Hall electric field on the r–z plane can be obtained by applying the magnetic field. The strong Hall electric field produces the large azimuthal component of electric current density. The interaction between the azimuthal component of electric current and the magnetic field pushes the shock wave away from OREX. As a result, the total aerodynamic heating can be reduced by about 70% of that obtained without applying the magnetic field under the present numerical flight conditions.

On the other hand, if the wall is the conducting wall, the large azimuthal component of electric current density cannot be produced because the strong Hall electric field cannot be obtained owing to

the existence of the paths of the electric current between the plasma in the shock layer and the conducting wall. Consequently, if the wall is the conducting wall the MHD control is not useful for controlling the flowfield and the aerodynamic heating.

Acknowledgments

This study was partly supported by Research Fellowships of the Japan Society for the Promotion of Science (JSPS) for Young Scientists and by the Grant-in-Aid for JSPS Fellow from the Ministry of Education, Culture, Sports, Science and Technology. A part of the computation in the present study was performed with the KDK system of the Research Institute for Sustainable Humanosphere at Kyoto University.

References

[1]Yamamoto, Y., "Recent Comparisons of Aerothermodynamic Results by CFD and FEM Coupling Analysis with OREX Flight Experiments," *Proceedings of the 13th NAL Symposium on Aircraft Computational Aerodynamics*, National Aerospace Lab. of Japan, Tokyo, 1995, pp. 27–39.

[2]Meyer, R. C., "On Reducing Aerodynamic Heat-Transfer Rates by Magnetohydrodynamic Techniques," *Journal of the Aero/Space Sciences*, Vol. 25, No. 9, 1958, pp. 561–566, 572.

[3]Bush, W. B., "Magnetohydrodynamic-Hypersonic Flow past a Blunt Body," *Journal of the Aero/Space Sciences*, Vol. 25, No. 11, 1958, pp. 685–690, 728.

[4]Ziemer, R. W., "Experimental Investigation in Magneto-Aerodynamics," *ARS Journal*, Vol. 29, No. 19, 1959, pp. 642–647.

[5]Yamamoto, A., "A Thin Superconducting Solenoid Magnet for Astroparticle Physics," *Nuclear Physics B* (Proc. Suppl.), Vol. 113, Dec. 2002, pp. 299–302.

[6]Fujino, T., Funaki, I., Sugita, H., Mizuno, M., and Ishikawa, M., "Numerical Analyses on Flow Control Around Blunt Body 'OREX' by Magnetic Field," AIAA Paper 2003-3760, June 2003.

[7]Porter, R. W., and Cambel, A. B., "Hall Effect in Flight Magnetogasdynamics," *AIAA Journal*, Vol. 5, No. 12, 1967, pp. 2208–2213.

[8]Lineberry, J. T., Bityurin, V. A., and Bocharov, A. N., "MHD Flow Control Studies Analytical Study of MHD Flow Interaction Around a Right Cylinder in Transverse Hypersonic Flow," AIAA Paper 2002-2112, May 2002.

[9]Takizawa, Y., Sato, S., Abe, T., and Konigorski, D., "Electro-Magnetic Effect on Shock Layer Structure in Reentry-Related High-Enthalpy Flow," AIAA Paper 2004-2162, June 2004.

[10]Kang, S. W., Jones, W. L., and Dunn, M. G., "Theoretical and Measured Electron-Density Distributions at High Altitudes," *AIAA Journal*, Vol. 11, No. 2, 1973, pp. 141–149.

[11]Park, C., "Assessment of Two-Temperature Kinetic Model for Ionizing Air," *Journal of Thermophysics and Heat Transfer*, Vol. 3, No. 3, 1989, pp. 233–244.

[12]Gnoffo, P. A., Gupta, R. N., and Shinn, J. L., "Conservation Equations and Physical Models for Hypersonic Air Flows in Thermal and Chemical Nonequilibrium," NASA TP-2867, Feb. 1989.

[13]Millikan, R. C., and White, D. R., "Systematics of Vibrational Relaxation," *Journal of Chemical Physics*, Vol. 39, No. 12, 1963, pp. 3209–3213.

[14]Wada, Y., and Liou, M.-S., "A Flux-Splitting Scheme with High-Resolution and Robustness for Discontinuities," AIAA Paper 94-0083, Jan. 1994.

[15]Yamamoto, S., "Shock-Vortex Capturing Method and Its Application to Unsteady 3-D Cascade Flow," *Computational Fluid Dynamics Journal*, Vol. 8, No. 2, 1999, pp. 341–349.

[16]Yoon, S., and Jameson, A., "Lower-Upper Symmetric-Gauss–Seidel Method for the Euler and Navier–Stokes Equations," *AIAA Journal*, Vol. 26, No. 6, 1988, pp. 1025, 1026.

[17]Eberhardt, S., and Imlay, S., "Diagonal Implicit Scheme for Computing Flows with Finite Rate Chemistry," *AIAA Journal*, Vol. 6, No. 2, 1992, pp. 208–215.

[18]Lobb, R. K., "Experimental Measurement of Shock Detachment Distance on Spheres Fired in Air at Hypervelocities," *The High Temperature Aspects of Hypersonic Flow*, edited by W. C. Nelson, Pergamon, New York, 1964, pp. 519–527.

[19]Yuhara, M., Fujino, T., and Ishikawa, M., "Numerical Analysis of Effects of Liquid Particles on Plasmadynamics in a Large-Scale Pulsed MHD Generator," AIAA Paper 2004-2369, June 2004.

I. Boyd
Associate Editor